Applied Catalysis B: Environmental 182 (2016) 266–276

Contents lists available at ScienceDirect

Applied Catalysis B: Environmental

journal homepage: www.elsevier.com/locate/apcatb

On the role of metal particle size and surface coverage for photo-catalytic hydrogen production: A case study of the Au/CdS system

I. Majeed [a], M. Amtiaz Nadeem [a,b,**], M. Al-Oufi [b], M. Arif Nadeem [a], G.I.N. Waterhouse [c], A. Badshah [a], J.B. Metson [c], H. Idriss [b,d,*]

[a] Department of Chemistry and Department of Environmental Sciences, Quid-i-Azam University, Islamabad 4200, Pakistan
[b] SABIC-Corporate Research and Development (CRD) at KAUST, Thuwal 23955, Saudi Arabia
[c] School of Chemical Sciences, University of Auckland, Private Bag 92019 Auckland, New Zealand
[d] Department of Chemistry, University College London, London WC1H 0AJ, UK

ARTICLE INFO

Article history:
Received 5 March 2015
Received in revised form 9 September 2015
Accepted 18 September 2015
Available online 25 September 2015

Keywords:
Au-CdS
Photo-catalytic hydrogen production
Metal particle agglomeration
Visible light irradiation
Ethanol–water splitting

ABSTRACT

Photo-catalytic hydrogen production has been studied on Au supported CdS catalysts under visible light irradiation in order to understand the effect of Au particle size as well as the reaction medium properties. Au nanoparticles of size about 2–5 nm were deposited over hexagonal CdS particles using a new simple method involving reduction of Au^{3+} ions with iodide ions. Within the investigated range of Au (between 1 and 5 wt.%) fresh particles with mean size of 4 nm and XPS Au4f/Cd3d surface ratio of 0.07 showed the highest performance (ca. 1 molecule of H_2/Au_{atom} s^{-1}) under visible light irradiation (>420 nm and a flux of 35 mW/cm^2). The highest hydrogen production rate was obtained from water (92%)-ethanol (8%) in an electrolyte medium (Na_2S–Na_2SO_3). TEM studies of fresh and used catalysts showed that Au particle size increases (almost 5 fold) with increasing photo-irradiation time due to photo-agglomeration effect yet no sign of deactivation was observed. A mechanism for hydrogen production from ethanol–water electrolyte mixture is presented and discussed.

© 2015 Elsevier B.V. All rights reserved.

1. Introduction

The effective use of solar energy is important for the establishment of a sustainable economy. Apart from solar energy utilization using photovoltaic technology and direct solar heating, one approach of solar energy utilization is the use of sunlight to generate energy carriers such as hydrogen from renewable sources (water or water/bio-ethanol mixture where the latter is used in small amounts to quench e–h recombination rates) using semiconductor photo-catalysts [1,2]. Moreover, ethanol can be synthesized from biomass, e.g., fermentation or hydrolyses of celluloses and this is not the case for other fossil fuels [3]. One of the important challenges to realize this is the development of photo-catalysts which can absorb sunlight and convert these renewables to hydrogen with efficiency that warrant scaling up of the process. A range of catalysts from simple binary metal oxides and metal sulfides to more complicated catalysts have been developed to achieve this objective [4–6]. TiO_2 [7–13] and CdS [14–18] attract special interest in this regard because of the relative simplicity of their chemical structure in addition to their stability.

TiO_2 is one of the most stable and active photo-catalyst known, [6,13,18,19] though it suffers from the limitation of its light absorption range mostly in the UV region of solar spectrum (anatase E_g = 3.2 eV, rutile E_g = 3.0 eV). This leaves ca. 95% of incoming sunlight not utilized. On the other hand, CdS has narrower band gap (E_g = 2.4 eV) allowing for visible light absorption below 515 nm (20–25% of the solar spectrum) [15,16]. CdS has two different stable structures; cubic and hexagonal. It has been recognized early on, that the hexagonal structure is far more active than the cubic one [20] despite the fact that both have a direct bang-gap [21]. However, CdS suffers from the limitation of its own oxidation by valence band holes produced during the photoexcitation process [22,23]. This problem is circumvented by introducing sacrificial agents with higher redox potential than the valence band of CdS

* Corresponding author at: Department of Chemistry, University College London, London WC1H 0AJ, UK.
** Corresponding author at: Department of Chemistry and Department of Environmental Sciences, Quid-i-Azam University, Islamabad 4200, Pakistan.
E-mail addresses: NadeemMI@SABIC.com (M.Amtiaz Nadeem), IdrissH@SABIC.com, h.idriss@ucl.ac.uk (H. Idriss).

http://dx.doi.org/10.1016/j.apcatb.2015.09.039
0926-3373/© 2015 Elsevier B.V. All rights reserved.

to prevent it from being oxidized. The process can be represented by the equations given below.

$$(Cd^{2+}S^{2-}) + h\nu(< 515\,nm) \rightarrow (Cd^{2+}S^{2-}) + e + h(\text{Excitation}) \quad (1)$$

$$(Cd^{2+}S^{2-}) + e + h + R \rightarrow Cd^{2+} + S^{-} + R^{-}(\text{Photocorrosion}) \quad (2)$$

$$(Cd^{2+}S^{2-}) + e + h + R + SA \rightarrow (Cd^{2+}S^{2-}) + R^{-} + SA_{ox}(\text{Photocatalysis}) \quad (3)$$

where R represents an electron acceptor species and SA represents a sacrificial agent.

CdS can either be used in presence of metals as electron traps [24] or coupled with other semiconductors to prevent electron-hole recombination [25,26]. Other catalyst fabrication methods, have shown improved CdS based catalysts, especially core shell structures with other stable semiconductors, with the objective to overcome the inherent photo-corrosion of CdS [27]. CdS has usually been coupled with noble metals such as Au, Pt, Rh, Ru and Pd acting as co-catalyst [28–31].

Several researchers have focused on CdS modification with other metal sulfides (WS_2, MoS_2) which has shown improved photo-catalytic activity as compared to CdS alone [32,33]. CdS nanoparticles are often incorporated within a layered metal oxides to suppress particle growth and formation of nano-hetero-junctions which quickly transfer electrons through the nanostructure while the recombination between the photo-induced electron and the hole is effectively suppressed [34–37]. Three component nano-junctions (CdS–Au–TiO_2) mimicking the natural photosynthesis has also been designed and tested [38,39]. CdS/TiO_2 nanotubes where the former is incorporated into the later has been demonstrated to show higher activity as compared to CdS alone [25]. CdS (core)-TiO_2 (shell) structure were also studied and has shown to possess up to seven times higher photo-catalytic activity as compared to CdS [40–42]. Graphene regarded as an ideal conductive material for nanoparticles forming hybrid structure with CdS has also shown up to five times enhancement in the photo-catalytic activity [43–45].

In the case of TiO_2, charge carriers are more stable in anatase than in rutile and thus partially explain the activity of the former [46]. There are no data available in the case of pure CdS linking charge carrier life time to structural and catalytic performance. Although in some cases semiconductors alone have been found to exhibit photo-catalytic activity, however in most studies metals have been found to increase the photo-catalytic activity considerably [47]. Metals (e.g., Pt, Pd, Ru, Rh and Au) are generally effective for facilitating H_2 evolution as a result of the H^+ reduction. Au has recently been the preferred co-catalyst for water splitting because it is less active for back reaction of H_2 oxidation,[48] have suitable work function [49] and is highly resistant to oxidation [50]. Moreover, under visible light irradiation, electrons can be transferred from Au particles to the conduction band of the semiconductor due to surface plasmon resonance which could be responsible for visible water splitting [51]. Au can also enhance the activity via plasmon resonance energy transfer rather than hot electron transfer where in this case both increase in charge carriers (because CdS and Au absorption overlap) and a decrease in charge carrier recombination rate could occur [52]. Au/CdS (hexagonal phase) photo-catalysts were thus selected as the main focus of this study.This study focuses on the effect of Au loading and the nature of the aqueous media on the enhancement of photo-catalytic activity. To the best of our knowledge, there are only three studies reported about Au/CdS [53–55] while other metals were used for most other studies [55–61]. Almost all of these studies have been performed using inorganic electrolyte (0.1 M Na_2S, 0.02 M Na_2SO_3) as reaction medium. There is no work reported on hydrogen production from a mixture of an inorganic electrolyte and organic sacrificial agent, ethanol in our case. This study also probe into the catalyst structure after the reaction in order to probe into the restructuring of the material that has occurred.

2. Experimental

2.1. Catalyst preparation

CdS nanoparticles were synthesized by the sol–gel method using equimolar amounts of $Cd(NO_3)_2{\cdot}4H_2O$ (Sigma–Aldrich, ≥99.0%) and $Na_2S{\cdot}9H_2O$ (Kanto Chemicals, ≥95.5%). Briefly, 2.1 g of $Cd(NO_3)_2$ was dissolved in 50 mL of isopropanol in a beaker and stirred vigorously. After 45 min, 50 mL of an aqueous $Na_2S{\cdot}9H_2O$ solution (0.136 M) was added drop wise over a period of one hour using a burette. The mixture was further stirred for two hours. The orange precipitate obtained was vacuum-filtered, washed five times with water to remove surplus ions, and subsequently heat treated at different temperatures overnight in air or an inert atmosphere (N_2) with the aim of increasing the proportion of the more catalytically active hexagonal CdS phase (Table 1).

Au loading was performed using a novel and facile iodide reduction method [62]. Briefly, an aqueous solution of KI (15 mL, 5 mM, Sigma–Aldrich, ≥99.5%) was added to 0.1 g of CdS powder. The mixture was stirred vigorously to make homogeneous slurry. Appropriate amounts of an aqueous $HAuCl_4{\cdot}3H_2O$ solution (5 mM, Sigma–Aldrich, ≥99.999%) were added to the slurry to achieve the desired Au loading. The mixture was then sonicated for 20 min in an Elmasonic sonicator (80 watt, 50/60 Hz output frequency) until the purple color of iodine was visible. The reaction takes place as given below;

$$M^{n} + n\Gamma \rightarrow M + \frac{n}{2}I_2 \quad (4)$$

The slurry was immediately subjected to vacuum filtration and washed with excess water to remove unreacted anions and I_2. The Au/CdS powders obtained were dried at 110 °C overnight in air before characterization and photo-catalytic H_2 production tests.

2.2. Catalyst characterization

X-ray diffraction for CdS phase analysis was conducted using a D500 Siemens Diffractometer (300 kV). Diffraction patterns were recorded from 10° to 90° in 0.02° s^{-1} steps. CdS particle size deter-

Table 1
Effect of heat treatment on CdS nanoparticles prepared by the sol–gel method.

No.	Overnight heat treatment	CdS phase (XRD)	Crystallite size (XRD)	Surface area (BET)
1	100 °C, air	Cubic	–	34 $m^2\,g^{-1}$
2	200 °, air	Cubic	13 nm	35 $m^2\,g^{-1}$
3	300 °C, air	Cubic	14 nm	35$m^2\,g^{-1}$
4	400 °C, air	Cubic	15 nm	32 $m^2\,g^{-1}$
5	500 °C, air	$CdSO_4$ white powder	–	–
6	600 °C, N_2 flow	Hexagonal phase	112 nm	5 $m^2\,g^{-1}$
7	800 °C, N_2 flow	Hexagonal phase	224 nm	1 $m^2\,g^{-1}$

mination and monitoring of Au loading was performed using Philips CM12/STEM Electron Microscope, PW 6030 (120 kV). BET surface area measurements were performed using a Micromeritics Tristar 300 Surface Area and Porosity Analyzer. UV–vis Spectra were recorded using a Shimadzu double–beam UV–2100 Spectrophotometer equipped with an integrating sphere, having a 60 mm internal diameter. Au/CdS and CdS samples spectra were recorded in the range of 250–900 nm at a slit width of 2 nm. The baseline correction was performed using $BaSO_4$ as the reference. X-ray photoelectron spectra (XPS) were collected on a Kratos Axis Ultra spectrometer using monochromatized Al Kα X-ray (hv = 1486.6 eV). The binding energy scale was calibrated using adventitious hydrocarbon referencing (C1s = 285.0 eV). The surface chemical states of the elements present were determined from narrow scan spectra taken at pass energy 20 eV over the C 1s, O 1s, and S 2p, Au 4f and Cd 3d regions (30 sweeps/150 ms dwell time). The raw XPS data was deconvoluted using Casa XPS peak fitting software using a Shirley background for C 1s, O 1s, S 2p and Au 4f peaks whilst a Tougaard background was used for the Cd 3d peaks because Shirley background could not be applied due to linear background between Cd $3d_{3/2}$ and Cd $3d_{5/2}$ peaks.

2.3. Catalytic testing

Photoreactions over the Au/CdS were conducted in ethanol, water electrolyte (0.1 M Na_2S, 0.02 M Na_2SO_3; pH 13) and a mixture of both at a total volume of 25 mL in a 105 mL Pyrex reactor. Initial tests were conducted in which catalysts amounts were changed (0.005, 0.01, and 0.02 g). Maximum H_2 production rate was obtained with 0.01 g (Supplementary Fig. A. 1). We have, therefore, carried out the tests at this catalyst concentration (0.4 g/L_{Liquid}). The decrease in H_2 production rate with a further increase in catalyst amount might be related to shadowing of some of catalyst particles directly in front of the light source and is further explained in the Section 3. A 500 W Warrior WEHL halogen bulb lamp with irradiation flux of 35 mW cm^{-2} at a distance of ca. 30 cm from the reactor was used as a light source. Further details can be found in Supplementary Fig. A. 2. The mixture was continuously stirred with a magnetic stirrer and cooled with an electric fan to maintain a constant temperature of ca. 25 °C. Gas samples (1 mL) were taken after appropriate intervals typically 15–30 min with a gas tight syringe and analyzed using a Shimadzu Gas Chromatograph Model GC 2014 equipped with 1010 PLOT, Fused Silica Column (30 × 0.53 mm) and a TCD detector for H_2 measurement. Hydrogen quantification was performed using a calibration curve. The apparent quantum yield was calculated under similar photo-catalytic reaction condition using the following equation: [63]

$$\text{Apparent quantum yield} = \frac{\text{Number of } H_2 \text{ molecules produced} \times 2}{\text{Number of incident photons}} \times 100 \quad (5)$$

The lamp produced radiation within the 350–900 nm range. However, CdS with band gap of 2.4 eV can be excited only by radiations below ca. 520 nm. The lamp power was calculated using wavelength versus intensity curve (Supplementary Fig. A. 2) and by comparing the area under radiation capable of excitation with the total integrated area under curve.

3. Results and discussion

XRD results indicate that the as-prepared CdS crystallizes mainly in the cubic phase with <10% of the hexagonal phase (Fig. 1a). The cubic phase remains the dominant CdS one on heating in air up to 400 °C, while a further increase in temperature to 500 °C leads to complete oxidation to white $CdSO_4$ in less than one hour. However, heating the as-prepared cubic CdS at 600 °C in inert environment (ca. 120 mL/min of N_2 flow rate) prevented the oxidation of CdS to $CdSO_4$ and converted cubic CdS to its hexagonal structure [59]. The BET surface area was found equal to 33 ± 1.5 and 5 ± 0.4 m^2g^{-1} for cubic (as-prepared) and hexagonal phase (600 °C-annealed) respectively. Further effect of heat treatment details can be found in Table 1 and Supplementary Fig. A. 3.

TEM analysis (Fig. 1b and c) indicates a spherical particle shape for both cubic and hexagonal phases with an average particle size of 15 nm and 105 nm, respectively. DR-UV–vis spectroscopy showed the band gaps of the cubic and hexagonal CdS phases to be 2.2 eV and 2.35 eV, respectively [64]. The sharper absorption edge observed for the hexagonal phase is attributed to the higher crystallinity of this sample [65]. Defect states act as trap centers for charge carriers thereby increasing electron–hole recombination rates and thus lower the number of charge carriers available for reactions at the surface of CdS. Photo-catalytic hydrogen production tests were conducted on both phases. The hexagonal phase was found active while the cubic phase was found almost inactive (results not shown as the cubic phase showed very low activity and was considered almost inactive). This is further supported by even higher H_2 rates per unit surface area for hexagonal phase obtained at 800 °C compared to the one obtained at 600 °C (Supplementary Fig. A. 4). Phase transformation can also be behind the considerable change in reaction rate. Such is the case in TiO_2 for example where the anatase phase is found to be more active than the rutile phase [66,67].

Fig. 2(a–d) shows TEM images for various Au/CdS (hexagonal) photo-catalysts as a function of Au loading. The average Au nanoparticle size increased with Au loading in the 1-5 wt.% range. At loadings of 1, 3 and 5 wt.% Au, the mean particle sizes of Au metal were ca. 2.1 ± 0.5, 4 ± 1.6 and 4.5 ± 1.5 nm. Although average Au particle size was about the same in the case of 3 and 5 wt.% loading, however, there is a higher fraction of larger Au particles in the case of the 5 wt.% Au sample (graphs (e–f)). Figure (h) clearly shows the increase in Au plasmon peak with increasing Au wt.%. Au nanoparticles exhibit strong SPR absorption at around 520 nm [68]. The position of SPR absorption of Au depends on particle size, shape, as well as the medium surrounding them [69,70].javascript:void(0); In this case, the SPR absorption of Au is shifted towards longer wavelength with increasing Au loading. Such an extent of SPR red-shift is consistent with earlier studies [70]. The amount of Au loaded was measured independently by XRF analysis and was almost identical with the nominal loading (±0.2 wt.%).

XPS analysis (Fig. 3) of the as-prepared cubic CdS sample (3a) gave binding energies of 404.8 eV for Cd $3d_{5/2}$ and 161.8 eV for S 2p core level peaks, confirming the synthesis of pure CdS [71]. These binding energy values were unchanged following the temperature-induced transformation of cubic CdS to hexagonal CdS (spectra b). However, the FWHM of the Cd 3d peaks decreased after high temperature treatment, suggesting Cd 3d core hole lifetimes were longer for the hexagonal CdS. Core hole lifetime has an inverse relationship with the width of the peak in XPS measurement; FWHM = h/τ where τ is the core-hole life time and h is Plank's constant [72]. In addition core hole lifetimes reflect crystallinity and electrical conductivity in the samples, both of which are clearly higher for the hexagonal CdS phase here. Other studies have related this effect to static fluctuations in valence charges due to bond length and bond angle variations in amorphous materials thus decreasing the core hole life times as compared to their crystalline counterparts [73,74]. This was also reflected in the S 2p spectra, in which the S $2p_{1/2}$ and $2p_{3/2}$ peaks are well-resolved in the case of the hexagonal CdS sample but poorly resolved in the case of the cubic CdS sample. A binding energy of 84.1 eV for the Au $4f_{7/2}$ peak of the Au/CdS (hexagonal) sample indicates that Au is present in the metallic state. S:Cd ratios were found 0.91 and 0.85 for as pre-

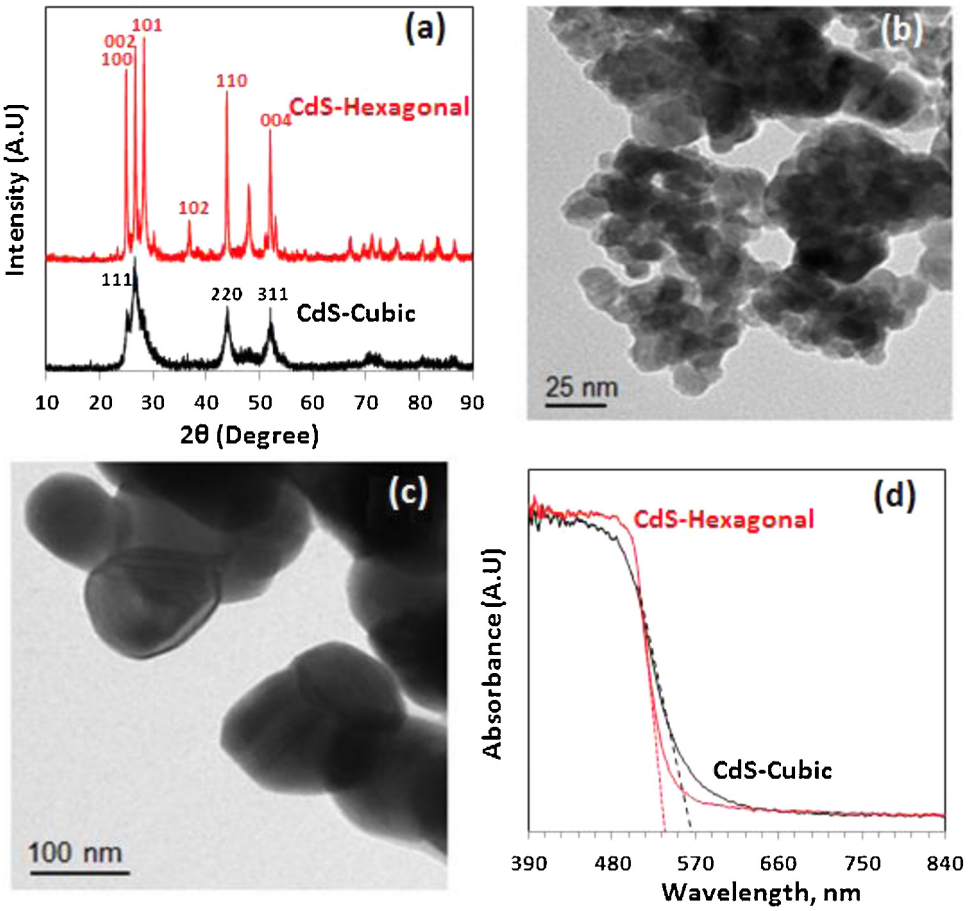

Fig. 1. (a) XRD of as-prepared cubic and hexagonal CdS obtained after heat treatment at 600 °C under N_2 flow; (b) TEM images of as-prepared cubic CdS and (c) hexagonal CdS; and (d) DR-UV–vis spectra of cubic CdS and hexagonal CdS.

Table 2
XPS data for the as-prepared cubic CdS, hexagonal CdS and an Au/CdS (hexagonal) sample.

Core Level	Position (eV) and [FWHM (eV)] Cubic Phase	Hexagonal phase
Cd $3d_{5/2}$	404.8 [1.37]	404.8 [0.91]
S $2p_{3/2}$	161.8 [1.21]	161.8 [0.85]
Au $4f_{7/2}$	–	84.1 [1.18]

pared and heat treated (600 °C under N_2) catalysts respectively. XPS results are summarized in Table 2.

Fig. 4 compares the H_2 production activity over a 3 wt.% Au/CdS photo-catalyst in ethanol, water electrolyte and ethanol–water electrolyte mixture. A weak H_2 production rate of ca. 23 μmol g^{-1} min^{-1} was found in pure ethanol or ethanol water system (volume ratio = 2:23), whilst no noticeable activity was observed in pure water (not shown due to extremely low hydrogen production rate as compared to others). The rate of hydrogen production of ca. 180 μmol g^{-1} min^{-1} with ethanol–water electrolyte mixture was found, (Fig. 4c) which is about two times higher than that obtained with water electrolyte alone (the most studied reactant system for CdS photo-catalysts) (Fig. 4b). The apparent quantum yield, based on the reactor configuration and the area of reactor exposed to light (13.93 cm^2) was found equal to 16.3%. The apparent quantum yield based on the complete radiation spectrum of the lamp was equal to ca. 4%. A comparison of hydrogen production rates with other catalysts is given in Table 3. It can be noticed that the 10 wt.%Pt/CdS with about three times higher metal loading is the only catalyst which has comparable activity to 3 wt.%Au/CdS used in this study.

Fig. 5 (a) shows the rate of H_2 production from an ethanol–water electrolyte mixture as a function of Au loading on CdS. Plots of hydrogen production versus time for these catalysts are presented in Supplementary Fig. A. 5. In Fig. 5 (b) the total number of Au particles were calculated from the mean size of Au particles present on Au/CdS using TEM images and the Au metal atom size (1.44 Å). Surface coverage was calculated from the area covered by each individual particle within a given distribution of metal particles normalized to total number of particles at each loading assuming that the area covered by single metal particle will be equal to the area inside its circumference [75]. It can be noted that Au enhances the rate of hydrogen production up to a loading of 3 wt.% Au. This can be attributed to electrons photo-excited in CdS under visible light being trapped by Au particles due to the lower Fermi level of Au as compared to CdS. These trapped electrons are further transferred to surface H^+ to reduce them to H_2 [47]. Although this view has been challenged recently where the role of Au is proposed to only help in the hydrogen recombination rather than in electron trapping [76]. An increase in photo catalytic activity with increased Au loading might be related to the increase in the area of Au/CdS interface as indicated by Fig. 5b. A decrease in activity with Au loading above 3 wt.% is observed. The decrease in photo catalytic hydrogen production with further increasing metal deposition has been observed by many other workers for which no clear explanation is yet known [10–12,77,78]. Upon increasing of metal particle coverage, large fraction of the semiconductor surface may become unavailable for light adsorption. It can also

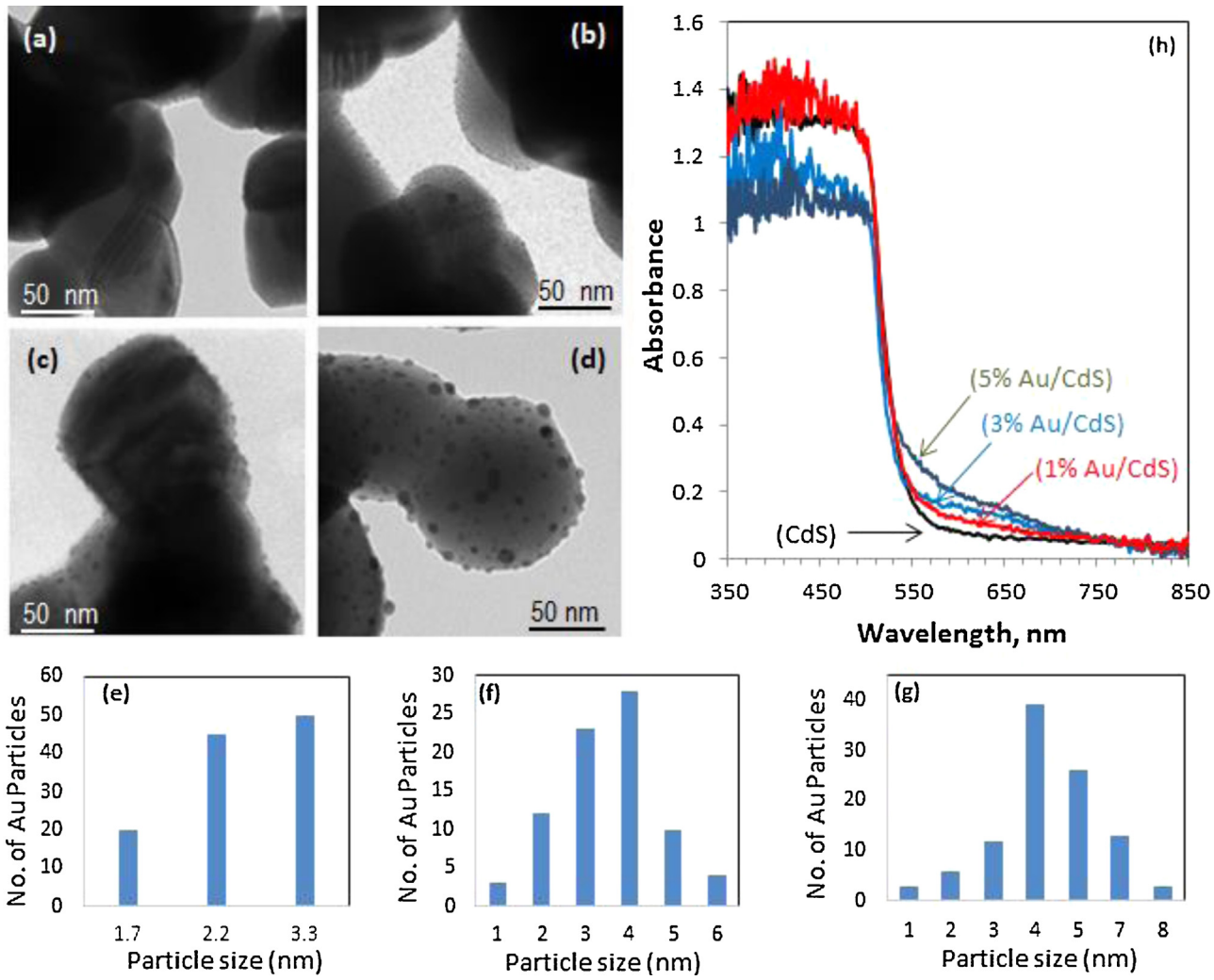

Fig. 2. TEM images of (a) hexagonal CdS; (b) 1 wt.% Au/CdS; (c) 3 wt.% Au/CdS; and (d) 5 wt.% Au/CdS with corresponding Au particle size distribution indicated by graphs (e), (f) and (g) respectively. Fig. (h) presents the DR-UV–vis spectra of catalysts as indicated. The average Au nanoparticle size increases with increasing Au loading.

Table 3
Hydrogen production over metal loaded CdS catalysts.

Metal loading and CdS morphology	Sacrificial agent	Irradiation used	H_2 production ($\mu mol\, g^{-1}\, min^{-1}$)	Year & Ref.
3 wt.% Au/CdS (Hexagonal nanoparticles)	Ethanol (8%)/0.1 M Na_2S; 0.02 M Na_2SO_3–(92%)	500 W Halogen lamp; Cut-off Filter = 420 nm	180	Present study
1 wt.% Au/CdS	0.25 M Na_2S; 0.35 M Na_2SO_3	300 W Xe lamp; Cut-off Filter = 420 nm	66	2012 [53]
CdS-shell@Au-core (44 wt.%)	0.1 M Na_2S; 0.1 M Na_2SO_3	300 W Xenon lamp; Cut-off Filter = 420 nm	3	2014 [54]
1 wt.% Pt/CdS hexagonal nanoparticles	0.24 M Na_2S; 0.35 M Na_2SO_3	400 W Hg lamp (UV)	98	2006 [56]
1.5 wt.% Pt/CdS (Hexagonal nanoparticles & nanorods)	Water (94%); Formic acid (6%)	400 W High-pressure Hg lamp; Cut-off Filter = 420 nm	17	2008 [57]
3 wt.% Pt/CdS (Hexagonal nanoparticles)	0.25 M Na_2S; 0.3 M Na_2SO_3	300 W Xenon lamp; Cut-off Filter = 420nm	32	2007 [58]
0.3 wt.% Pt/CdS (Cubic & hexagonal)	0.1 M Na_2S; 0.02 M Na_2SO_3/1 M NaOH	High-pressure Hg-Xenon arc lamp; Cut-off Filter = 400 nm	11	2008 [59]
1wt%. Pt/CdS (Cubic)	0.01 M Na_2S; 0.015 M Na_2SO_3	160 W Hg lamp	13.8	2009 [60]
10 wt.% Pt/CdS (Hexagonal Nanorods and sheet)	0.25 M Na_2S; 0.35 M Na_2SO_3	300 W Xenon lamp; Cut-off Filter = 420 nm	229	2008 [61]
2 wt.% Au/-2 wt.% Pt/CdS (Hexagonal)	0.05 M Na_2S; 0.1 M Na_2SO_3	300 W Xenon lamp; Cut-off Filter = 420 nm	50	2011 [55]

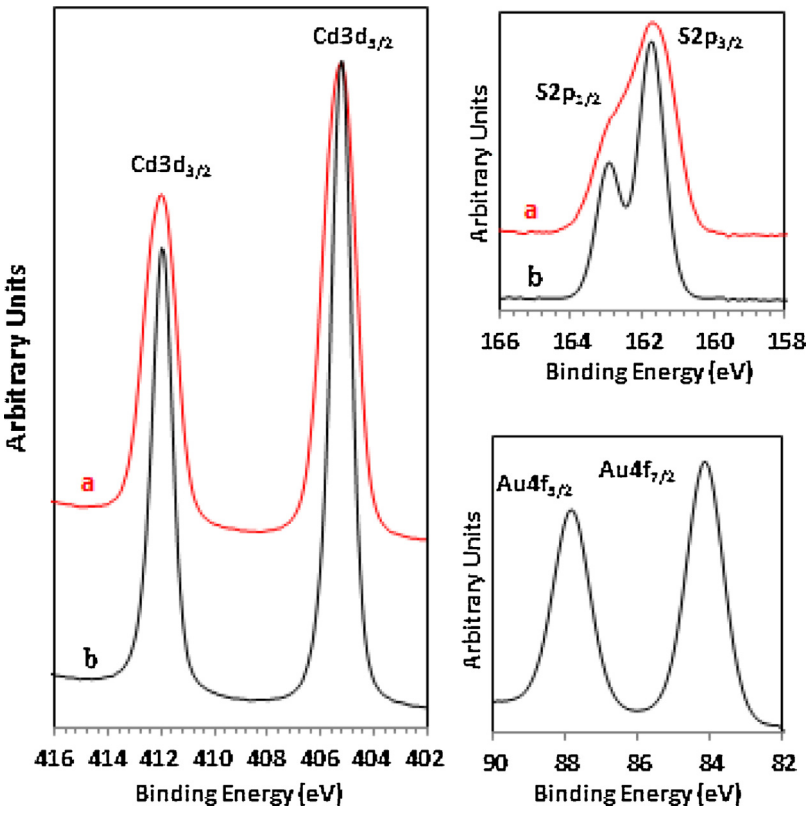

Fig. 3. X-ray photoelectron spectra of the Cd 3d, S 2p and Au 4f regions for (a) as-prepared cubic CdS; and (b) ripened hexagonal CdS and 5 wt.% Au/CdS (hexagonal) sample.

Table 4
Rate of photo catalytic H_2 production rates and TOF (s^{-1}) from water–ethanol electrolyte over Au/CdS as a function of Au loading. Hexagonal CdS; BET surface area = 5 m^2/g_{Catal} (Table 1).

Au (wt.%)	Mean Au particle size (nm)	XPS Au 4f/Cd 3d (At.%)	H_2 production rate 10^{-6} mol $g^{-1}{}_{Catal} \times s^{-1}$	TOF H_2 production rate molecules $Au^{-1}{}_{atom}$ s^{-1}
0	–	–	0.17	–
1	2.0 ± 0.34	0.032	1	0.8
3	4.0 ± 1.6	0.076	3	1
5	4.5 ± 1.5	0.121	1	0.2

result in increasing surface defects at metal-semiconductor interface leading to an increase in electron-hole recombination centres. The hydrogen production rates for the different Au/CdS catalysts are listed in Table 4. The third column contains the corrected XPS Au 4f/Cd 3d peak area ratios for Au/Cd. The last column shows the reaction rate in molecules/(Au_{atom} s^{-1}) (considering that 1 m^2 contains ca. 5×10^{18} atoms of Cd or S). The number of Au atoms were calculated by multiplying XPS Au/4f/Cd 3d ratio (column 3) with total number of Cd or S atoms in a given surface area. The following formula was used to obtain TOF.

$$\mathrm{TOF} = \frac{[\mathrm{H_2\ rate\ (mol\,g^{-1}s^{-1})}] \times [\mathrm{Avogadro's\ No\ (Number\ of\ molecules\ mol^{-1})}]}{[\mathrm{XPS\ Au4f/Cd3d\ at.\%\ ratio}] \times [\mathrm{BET\ surface\ area\ (m^2g^{-1})}] \times [\mathrm{Number\ of\ Cd\ or\ S\ atoms\ (m^{-2})}]}$$

Increasing the wt.% from 1 to 3% resulted in increasing the hydrogen production by about the same factor per unit mass. The nominal rate per Au atom increased by ca. 25% (from 0.8 to 1 s^{-1}) while the surface coverage increased by 2.3 times [(0.076/0.032)]. Increasing the amount of Au did not substantially increase its dispersion but made larger particles instead (Fig. 2b and c). Still the increase of the rate with increasing Au wt.% together with increasing particle size may indicate that on CdS larger particles of Au (≈4–6 nm) are either as active as smaller particles (≈2–3 nm) or slightly more active (last column in Table 4). This result may indicate that the role of Au might be (in addition to acting as electron sink) linked to the electric field generated upon illumination; due to its plasmonic resonance. In other words, the larger the particle size, the larger is the local electric field. Wang et al. very recently calculated that a local field enhancement factor $|E|^2/|E_o|^2$ of 5.3 can be obtained for Au/Fe_2O_3 system with Au particle size in 13–20 nm range with respect to Au particle size in 3.5–13 nm range [79]. This also indicates the absence of appreciable influence of hot electrons in the catalytic reaction as production of hot electrons is dominant process for smaller nanostructures [80–82]. This interpretation might be in line with energy transfer (not electron transfer) scheme recently proposed [52] and is more in line with the role of metals in photo-catalytic hydrogen production where electron transfer occurs from the conduction band to the metal and not the other way around [76].

A TEM study of the 5 wt.% Au/CdS photo-catalyst was undertaken to monitor the possible changes in the structure of the photo-catalyst during reaction (Fig. 6). It was opted to monitor the activity of a 5 wt.% Au/CdS instead of the 3 wt.% as it had larger

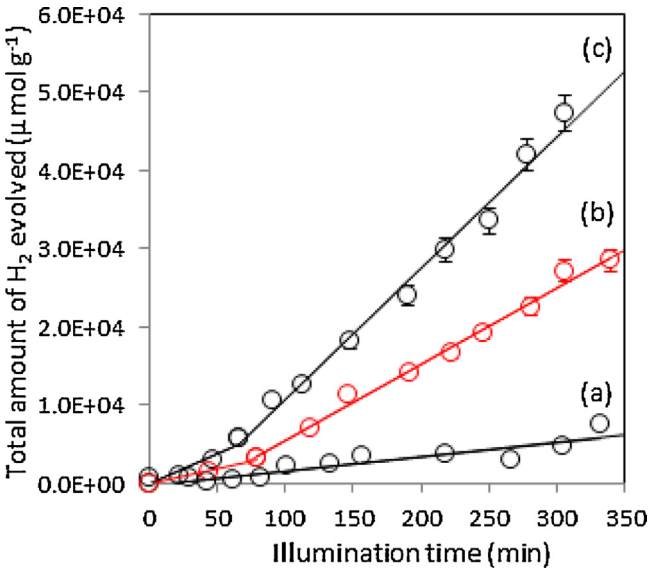

Fig. 4. Photo-catalytic H_2 production over 3 wt.% Au/CdS using; (a) ethanol, (b) water electrolyte and (c) ethanoldS Morphologywater electrolyte system in 2:23 volume ratio.

particle size making structural analysis less prone to errors. The as-prepared 5 wt.% Au/CdS photo-catalyst (Fig. 6, image a) had Au particle size distribution in the 1–8 nm range. Au particle size increased with increasing irradiation time, reaching a maximum size of ca. 20 nm after 80 min (Fig. 6, images b–d). After 90 min, steady H_2 production rate is obtained (Supplementary Fig. A 5d), after which the rate did not change significantly with continuous testing over further 4.5 h. Somef the catalysts were tested for longer periods of time to examine the effects of the sacrificial reagent concentration and surface corrosion. A decline in H_2 production rate was observed after 18 h due to a decrease in sacrificial agent concentration by ca. 70–80% which in turn may have resulted in enhanced surface corrosion indicated by the enhanced roughness of CdS particles surface (image 6d). However, if the concentration of the sacrificial agents is maintained, no change in catalytic activity is noticed on its re-use. The tendency of smaller Au particles to form larger ones at the start of the reaction may be due to the strong absorption of incoming light by Au nanoparticles (plasmon resonance) due to their larger number and subsequent conversion of light energy into thermal energy. This results in an increase in the local temperature which in turn accelerates particle diffusion and lead to agglomeration [83]. It has been reported that gold metal particles can become very hot when exposed to light in aqueous phase. A dramatic temperature jump (up to 465 K) has been observed as the nanoscale vapor layer formed on the particle surface thermally decouples the nanoparticle from the surrounding liquid [84,85]. The diffusion of Au on CdS single crystal has been noticed earlier and diffusion coefficient ($D = 3.33 \times 10^{-20}$ m^2 s^{-1} at 300 °C) has been calculated [86].

As the reaction proceeds, an increase in light absorption by CdS itself due to decrease in the Au particles density is expected. This results in enhanced probability of electron-hole pair generation. The electrons in the conduction band of CdS migrate onto Au particles, after some specific time ca. 70–90 min, an equilibrium is established and a constant rate of hydrogen production is observed as indicated in Supplementary Fig. A 5. This observation is in line with the results obtained as a function of a catalyst amount (Supplementary Fig. A. 1). With a fixed irradiation intensity and reactor configuration, a longer induction time will be expected as the catalyst amount is increased (i.e., more photo-catalyst means more photons will need to be supplied before light-induced surface aggregation of Au nanoparticles reach an equilibrium stage and a steady state reaction condition is achieved).

The increased hydrogen production rates using the ethanol–water electrolyte mixture can be explained by the reaction mechanism shown in Fig. 7. During the first step, the H_2O molecule is dissociated on the Cd–S surface to produce adsorbed Cd–OH and S–H species (step 1). Upon irradiation, electrons are promoted to the conduction band leaving holes in the valence band (step 2). A chemical reaction is initiated due to the reaction of aqueous S^{2-} ions (S^{2-}/S_2^{2-}; $E = -0.14$ eV versus NHE at pH = 7 [87]) with the valence band holes indicated by step 5 ($E = +1.7$ eV versus NHE at pH = 7 [88]). Subsequently, some of the electrons in the conduction band are trapped by Au particles on the surface (step 3) or migrated to the surface of CdS. These electrons are poised to reduce H^+ of surface OH groups to H_2 (step 4). In addition surface OH groups adsorbed on Cd atoms can react with the holes in the valence band to produce OH radicals [89]. CdS surface can be regarded mainly as comprising nonpolar $(11\bar{2}0)$ and $(10\bar{1}0)$ faces both of which have equal number of Cd and S atoms [90–92]. Ethanol may react with these OH radicals to

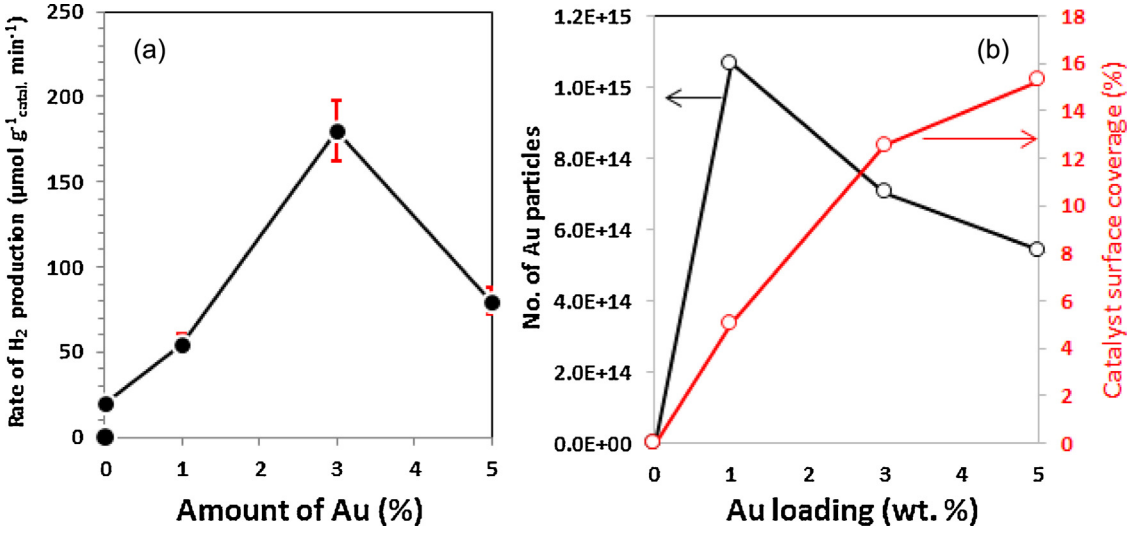

Fig. 5. Rate of photo-catalytic H_2 production from ethanol and water electrolyte mixture (8:92) over Au/CdS as a function of Au loading. Fig. 5 (b) presents the total number of Au particles and% of catalyst surface area covered for 0.01 g of catalyst as a function of Au loading.

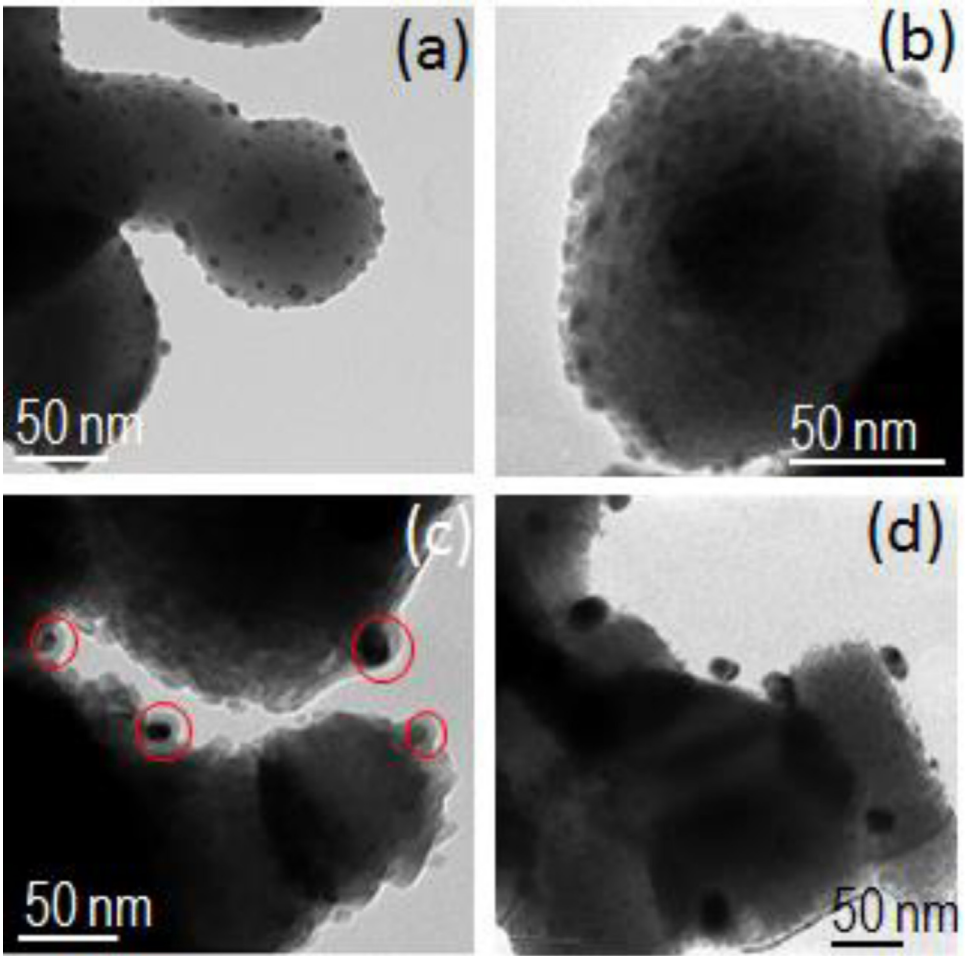

Fig. 6. TEM images of a 5 wt.% Au/CdS photo-catalyst at various stages of the photoreaction; (a) before photoreaction, after (b) 30 min, (c) 90 min and (d) 24 h. Au nanoparticle size increases with increasing irradiation time.

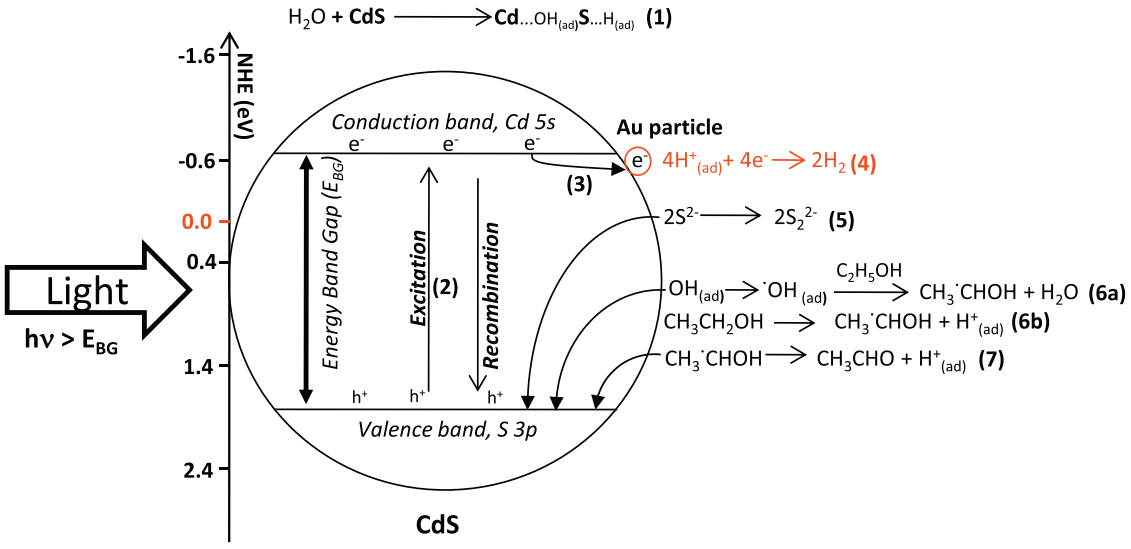

Fig. 7. Schematic representation of the mechanism for hydrogen production from ethanol–water electrolyte mixture on Au supported CdS catalysts.

produce α-hydroxyethyl radical and protonate the adsorbed OH to produce water (step 6a). Ethanol may also react directly with the holes to give the same intermediate and a proton (step 6b). This α-hydroxyethyl radical (E = +1.38 at pH = 7 eV versus NHE [93]) further reacts with a hole in the valence band to produce acetaldehyde and a proton (step 7). These protons produced are converted to gaseous hydrogen by the trapped electrons on Au (step 1). There was negligible reaction for Au/CdS in water or ethanol under visible light irradiation (Supplementary Fig. A. 6). This implies that the first step is the reaction of valence band holes with the sulfide

sacrificial agent enabling conduction band electrons to migrate onto Au particles or the surface of CdS and react with surface H^+ to give H_2. However, the α-hydroxyethyl radical produced also acts as a hole scavenger once the reaction has started thus producing acetaldehyde and H^+ ions. This results in increased hydrogen production rates and consequently reduces the amount of sulfide sacrificial agent consumed. Acetaldehyde production in the gas phase was monitored and presented in Supplementary Fig. A.6. It is worth noting that acetaldehyde is a reaction intermediate as it will (like most oxygen containing organic compounds) react to give further products that ultimately result in CO_2 (the final thermodynamic compound for organic oxidation). The reaction of gas phase acetaldehyde was studied under photo-irradiation over TiO_2 (110) single crystal [94], TiO_2 powder [95] but we are not aware of reported reaction on CdS in alkaline environment. One of the properties of acetaldehyde is its fast oxidation to acetate/acetic acid in presence of oxygen. One of the authors has previously shown that acetates/acetic acid react on TiO_2 via the photo-Kolbe reaction to give CH_4, C_2H_6 and CO_2 [96,97]. These products were looked for in this work but were not found. The low miscibility of CH_4 and C_2H_6, and their relative stability, in the liquid phase at room temperature would make their detection possible if they are formed. In other words, their absence in the gas phase indicates that this pathway is not favored on CdS at the present experimental conditions. Yet for CO_2 the situation is more complex because of its high solubility in the alkaline medium. This high solubility, associated with the expected small concentration, is probably the reason why it is not seen in the gas phase. Most likely the reaction would follow a photo-reforming, which is analogous to thermal reforming ($CH_3CHO + 3H_2O \rightarrow 5H_2 + 2CO_2$) and this would explain the increase in hydrogen production rate.

4. Conclusions

Au nanoparticles deposited on CdS by reductive deposition method with KI were prepared and used as a model to test the metal particle size activity as well as the effect of reaction medium. Mean particles sizes between 2 nm to 5 nm were obtained by changing the initial nominal Au wt.% (from 1 to 5 wt.%). The crystallinity of the Au/CdS photo-catalyst monitored by XRD could also be monitored by S 2p and Cd 3d XPS core levels where a decrease in the FWHM of 0.5 eV for Cd 3d and 0.4 eV for S2p for the high crystalline semiconductor is noticed and explained as due to increasing the core hole life time in the crystalline phase. The optimum rate for hydrogen production was found for particles with initial mean particle size of 4 nm. Prolonged photo-catalytic reaction time resulted in further increase in particle size up to 20 nm without noticeable decrease in catalytic reactivity. This latter results indicate that particle size might not be a determining factor in this system. This work supports the electron transfer mechanism from semiconductor to metal which may further be facilitated by metal to semiconductor energy transfer mechanism due to Au surface plasmon resonance. The addition of ethanol to the electrolyte (Na_2S/Na_2SO_3) further increased the production of hydrogen via additional injection of electrons into the valence band allowing for more H^+ to be reduced.

Acknowledgments

This work was conducted under the financial support of Uniservices Ltd, University of Auckland, New Zealand and the Higher Education Commission of Pakistan. We would like to thank Morgan Allison for his assistance in the laboratory work.

Appendix A. Supplementary data

Supplementary data associated with this article can be found, in the online version, at http://dx.doi.org/10.1016/j.apcatb.2015.09.039.

References

[1] M. Ni, M.K.H. Leung, K. Sumathy, D.Y.C. Leung, Potential of renewable hydrogen production for energy supply in Hong Kong, Int. J. Hydrogen Energy 31 (2006) 1401–1412.
[2] A. Haryanto, S. Fernando, N. Murali, S. Adhikari, Current status of hydrogen production techniques by steam reforming of ethanol: a review, Energy Fuels 19 (2005) 2098–2106.
[3] M.A. Nadeem, K.A. Connelly, H. Idriss, The photoreaction of TiO_2 and Au/TiO_2 single crystal and powder with organic adsorbates, Int. J. Nanotechnol. 9 (2012) 121–162.
[4] A. Kudo, H. Kato, I. Tsuji, Strategies for the development of visible-light-driven photocatalysts for water splitting, Anglais 33 (2004) 1534–1539.
[5] S. Padikkaparambil, Y. Zahira, S. Viswanathan, B. Njarakkattuvalappil, A. Zubair, An enthusiastic glance in to the visible responsive photocatalysts for energy production and pollutant removal, with special emphasis on titania, Int. J. Photoenergy 2012 (2012) 19.
[6] A. Kudo, Y. Miseki, Heterogeneous photocatalyst materials for water splitting, Chem. Soc. Rev. 38 (2009) 253–278.
[7] S. Bashir, A.K. Wahab, H. Idriss, Synergism and photocatalytic water splitting to hydrogen over Pt/TiO_2 catalysts: Effect of particle size, Catal. Today 240 (2015) 242–247.
[8] A.K. Wahab, M. Al-Oufi, S. Bashir, Y. Al-Salik, H. Katsiev, H. Idriss, Photocatalyst, method of preparation, photolysis system, World Patent 13T&I0037-WO-PCT (2013).
[9] G.I.N. Waterhouse, A.K. Wahab, M. Al-Oufi, V. Jovic, D.H. Anjum, D. Sun-Waterhouse, J. Llorca, H. Idriss, HYdrogen production by tuning the photonic band gap with the electronic band gap of TiO_2, Sci. Rep. 3 (2013) 2849.
[10] W.-T. Chen, H. Idriss, G.I.N. Waterhouse, Efficient photocatalytic H_2 production from ethanol–water mixtures over CuO/TiO_2 photocatalysts, Int. J. Hydrogen Energy 38 (2013) 15036–15048.
[11] V. Jovic, W.-T. Chen, D. Sun-Waterhouse, M.G. Blackford, H. Idriss, G.I.N. Waterhouse, Effect of gold loading and TiO_2 support composition on the activity of Au/TiO_2 photocatalysts for H_2 production from ethanol–water mixtures, J. Catal. 305 (2013) 307–317.
[12] V. Jovic, Z.H.N. Al-Azria, D. Sun-Waterhouse, H. Idriss, G.I.N. Waterhouse, Photocatalytic H_2 production from bioethanol over Au/TiO_2 and Pt/TiO_2 photocatalysts under UV irradiation—A comparative study, Top. Catal. 56 (2013) 1139–1151.
[13] M. Al-Oufi, A.K. Wahab, S. Bashir, Y. Al-Salik, H Idriss, Photocatalytic hydrogen production from water over Ag-Pd-Au deposited on titanium dioxide materials, US Patent (13T&I0023-US-PSP) Serial Number 61/93724 (2014).
[14] X. Chen, W. Shangguan, Hydrogen production from water splitting on CdS-based photocatalysts using solar light, Front Energy 7 (2013) 111–118.
[15] S.Y. Ryu, W. Balcerski, T.K. Lee, M.R. Hoffmann, Photocatalytic production of hydrogen from water with visible light using hybrid catalysts of CdS attached to microporous and mesoporous silicas, J. Phys. Chem. C 111 (2007) 18195–18203.
[16] S. Datta, M. Kabir, T. Saha-Dasgupta, Effects of shape and composition on the properties of CdS nanocrystals, Phys. Rev. B 86 (2012) 115307.
[17] J.F. Reber, M. Rusek, Photochemical hydrogen production with platinized suspensions of cadmium sulfide and cadmium zinc sulfide modified by silver sulfide, J. Phys. Chem. 90 (1986) 824–834.
[18] J.S. Jang, W. Li, S.H. Oh, J.S. Lee, Fabrication of CdS/TiO_2 nano-bulk composite photocatalysts for hydrogen production from aqueous H_2S solution under visible light, Chem. Phys. Lett. 425 (2006) 278–282.
[19] O. Carp, C.L. Huisman, A. Reller, Photoinduced reactivity of titanium dioxide, Prog. Solid State Chem 32 (2004) 33–177.
[20] M. Matsumura, S. Furukawa, Y. Saho, H. Tsubomura, Cadmium sulfide photocatalyzed hydrogen production from aqueous solutions of sulfite: effect of crystal structure and preparation method of the catalyst, J. Phys. Chem. 89 (1985) 1327–1329.
[21] N. Soltani, E. Gharibshahi, E. Saion, Band gap of cubic and hexagonal CdS quantum dots-experimental and theoretical studies, Chalcogenide Lett. 9 (2012) 321–328.
[22] Y.V. Pleskov, Y.Y. Gurevich, Semiconductor Photoelectrochemistry, Consultants Bureau, New York, NY, 1986.
[23] D. Meissner, C. Benndorf, R. Memming, Photocorrosion of cadmium sulfide: analysis by photoelectron spectroscopy, Appl. Surf. Sci. 27 (1987) 423–436.
[24] X. W. Yao, C. Song, Q. Huang, Q. Wu Xu, Enhancing solar hydrogen production via modified photochemical treatment of Pt/CdS photocatalyst, Catal. Today 199 (2013) 42–47.
[25] C. Li, J. Yuan, B. Han, L. Jiang, W. Shangguan, TiO_2 nanotubes incorporated with CdS for photocatalytic hydrogen production from splitting water under visible light irradiation, Int. J. Hydrogen Energy 35 (2010) 7073–7079.
[26] J.S. Jang, S.M. Ji, S.W. Bae, H.C. Son, J.S. Lee, Optimization of CdS/TiO_2 nano-bulk composite photocatalysts for hydrogen production from

Na_2S/Na_2SO_3 aqueous electrolyte solution under visible light ($\lambda \geq 420$ nm), J. Photochem. Photobiol. A: Chem. 188 (2007) 112–119.
[27] L. Huang, X. Wang, J. Yang, G. Liu, J. Han, C. Li, Dual cocatalysts loaded type I CdS/ZnS Core/Shell nanocrystals as effective and stable photocatalysts for H_2 evolution, J. Phys. Chem. C 117 (2013) 11584–11591.
[28] N. Bao, L. Shen, T. Takata, K. Domen, A. Gupta, K. Yanagisawa, C.A. Grimes, Facile Cd-thiourea complex thermolysis synthesis of phase-controlled Cds nanocrystals for photocatalytic hydrogen production under visible light, J. Phys. Chem. C 111 (2007) 17527–17534.
[29] T.-T. Yang, W.-T. Chen, Y.-J. Hsu, K.-H. Wei, T.-Y. Lin, T.-W. Lin, Interfacial charge carrier dynamics in core–shell Au-Cds nanocrystals, J. Phys. Chem. C 114 (2010) 11414–11420.
[30] J. Yang, H. Yan, X. Wang, F. Wen, Z. Wang, D. Fan, J. Shi, C. Li, Roles of cocatalysts in Pt–PdS/CdS with exceptionally high quantum efficiency for photocatalytic hydrogen production, J. Catal. 290 (2012) 151–157.
[31] Y. M. Luo, J. Liu, H. Hu, J. Li Liu, One-pot synthesis of Cds and Ni-doped Cds hollow spheres with enhanced photocatalytic activity and durability, ACS Appl. Mater. Interfaces 4 (2012) 1813–1821.
[32] X. Zong, J. Han, G. Ma, H. Yan, G. Wu, C. Li, Photocatalytic H_2 evolution on cds loaded with WS_2 as cocatalyst under visible light irradiation, J. Phys. Chem. C 115 (2011) 12202–12208.
[33] X. Zong, G. Wu, H. Yan, G. Ma, J. Shi, F. Wen, L. Wang, C. Li, Photocatalytic H_2 evolution on MoS_2/CdS catalysts under visible light irradiation, J. Phys. Chem. C 114 (2010) 1963–1968.
[34] W. Shangguan, A. Yoshida, Photocatalytic hydrogen evolution from water on nanocomposites incorporating cadmium sulfide into the interlayer, J. Phys. Chem. B 106 (2002) 12227–12230.
[35] W. Shangguan, A. Yoshida, Synthesis and photocatalytic properties of CdS-intercalated metal oxides, Sol. Energy Mater. Sol. Cells 69 (2001) 189–194.
[36] X.-F. Gao, W.-T. Sun, Z.-D. Hu, G. Ai, Y.-L. Zhang, S. Feng, F. Li, L.-M. Peng, An efficient method to form heterojunction CdS/TiO_2 photoelectrodes using highly ordered TiO_2 nanotube array films, J. Phys. Chem. C 113 (2009) 20481–20485.
[37] D. Barpuzary, Z. Khan, N. Vinothkumar, M. De, M. Qureshi, Hierarchically grown urchinlike CdS@ZnO and CdS@Al_2O_3 heteroarrays for efficient visible-light-driven photocatalytic hydrogen generation, J. Phys. Chem. C 116 (2011) 150–156.
[38] H. Kato, M. Hori, R. Konta, Y. Shimodaira, A. Kudo, Construction of Z-scheme type heterogeneous photocatalysis systems for water splitting into H_2 and O_2 under Visible light irradiation, Anglais 33 (2004) 1348–1349.
[39] H. Tada, T. Mitsui, T. Kiyonaga, T. Akita, K. Tanaka, All-solid-state Z-scheme in CdS–Au–TiO_2 three-component nanojunction system, Nat. Mater. 5 (2006) 782–786.
[40] J. Cao, J.-Z. Sun, H.-Y. Li, J. Hong, M. Wang, A facile room-temperature chemical reduction method to TiO_2@CdS core/sheath heterostructure nanowires, J. Mater. Chem. 14 (2004) 1203–1206.
[41] K. Das, S. De, Optical properties of the type-ii core–shell TiO_2@CdS Nanorods for photovoltaic applications, J. Phys. Chem. C 113 (2009) 3494–3501.
[42] H. Jia, H. Xu, Y. Hu, Y. Tang, L. Zhang, TiO_2 CdS core–shell nanorods films: Fabrication and dramatically enhanced photoelectrochemical properties, Electrochem. Commun. 9 (2007) 354–360.
[43] J. Zhang, J. Yu, M. Jaroniec, J.R. Gong, Noble metal-free reduced graphene oxide-$Zn_xCd_{1-x}S$ nanocomposite with enhanced solar photocatalytic H_2-production performance, Nano Lett. 12 (2012) 4584–4589.
[44] P. Gao, J. Liu, S. Lee, T. Zhang, D.D. Sun, High quality graphene oxide-CdS-Pt nanocomposites for efficient photocatalytic hydrogen evolution, J. Mater. Chem. 22 (2012) 2292–2298.
[45] H. Lee, K. Heo, A. Maaroof, Y. Park, S. Noh, J. Park, J. Jian, C. Lee, M.-J. Seong, S. Hong, High-performance photoconductive channels based on (carbon nanotube)–(CdS nanowire) hybrid nanostructures, Small 8 (2012) 1650–1656.
[46] M. Xu, Y. Gao, E.M. Moreno, M. Kunst, M. Muhler, Y. Wang, H. Idriss, C. Wöll, Topological features of electronic band structure and photochemistry: new insights from spectroscopic studies on single crystal titania substrates, Phys. Rev. Lett. 106 (2011) 138302–138304.
[47] M. Murdoch, G.I.N. Waterhouse, M.A. Nadeem, J.B. Metson, M.A. Keane, R.F. Howe, J. Llorca, H. Idriss, The effect of gold loading and particle size on photocatalytic hydrogen production from ethanol over Au/TiO_2 nanoparticles, Nat. Chem. 3 (2011) 489–492.
[48] M. Haruta, Size and support dependency in the catalysis of gold, Catal. Today 36 (1997) 153–166.
[49] P. Gomathisankar, D. Yamamoto, H. Katsumata, T. Suzuki, S. Kaneco, Photocatalytic hydrogen production with aid of simultaneous metal deposition using titanium dioxide from aqueous glucose solution, Int. J. Hydrogen Energy 38 (2013) 5517–5524.
[50] T. Sreethawong, S. Yoshikawa, Comparative investigation on photocatalytic hydrogen evolution over Cu, Pd, and Au-loaded mesoporous TiO_2 photocatalysts, Catal. Commun. 6 (2005) 661–668.
[51] Y. Tian, T. Tatsuma, Mechanisms and applications of plasmon-induced charge separation at TiO_2 Films loaded with gold nanoparticles, J. Am. Chem. Soc. 127 (2005) 7632–7637.
[52] R. Amrollahi, M.S. Hamdy, G. Mul, Understanding promotion of photocatalytic activity of TiO_2 by Au nanoparticles, J. Catal. 319 (2014) 194–199.
[53] S. P. Shen, D. Zhao, Y. Su, A. Orlov Li, Outstanding activity of sub-nm Au clusters for photocatalytic hydrogen production, Appl. Catal. B 126 (2012) 153–160.
[54] X. Ma, K. Zhao, H. Tang, Y. Chen, C. Lu, W. Liu, Y. Gao, H. Zhao, Z. Tang, New insight into the role of gold nanoparticles in Au@ CdS core–shell nanostructures for hydrogen evolution, Small 10 (2014) 4664–4670.
[55] H.J. Yun, H. Lee, N.D. Kim, D.M. Lee, S. Yu, J. Yi, A combination of two visible-light responsive photocatalysts for achieving the Z-scheme in the solid state, ACS Nano 5 (2011) 4084–4090.
[56] M. Sathish, B. Viswanathan, R. Viswanath, Alternate synthetic strategy for the preparation of CdS nanoparticles and its exploitation for water splitting, Int. J. Hydrogen Energy 31 (2006) 891–898.
[57] Y. Li, J. Du, S. Peng, D. Xie, G. Lu, S. Li, Enhancement of photocatalytic activity of cadmium sulfide for hydrogen evolution by photoetching, Int. J. Hydrogen Energy 33 (2008) 2007–2013.
[58] N. Bao, L. Shen, T. Takata, K. Domen, A. Gupta, K. Yanagisawa, C.A. Grimes, Facile Cd-thiourea complex thermolysis synthesis of phase-controlled CdS nanocrystals for photocatalytic hydrogen production under visible light, J. Phys. Chem. C 111 (2007) 17527–17534.
[59] L.A. Silva, S.Y. Ryu, J. Choi, W. Choi, M.R. Hoffmann, Photocatalytic hydrogen production with visible light over Pt-interlinked hybrid composites of cubic-phase and hexagonal-phase CdS, J. Phys. Chem. C 112 (2008) 12069–12073.
[60] B. Girginer, G. Galli, E. Chiellini, N. Bicak, Preparation of stable CdS nanoparticles in aqueous medium and their hydrogen generation efficiencies in photolysis of water, Int. J. Hydrogen Energy 34 (2009) 1176–1184.
[61] N. Bao, L. Shen, T. Takata, K. Domen, Self-templated synthesis of nanoporous CdS nanostructures for highly efficient photocatalytic hydrogen production under visible light, Chem. Mater. 20 (2007) 110–117.
[62] A. Al-Ameer, H. Katsiev, L. Sinatra, I. Hussein, O.M. Bakr, Gold nanoparticle growth control—implementing novel wet chemistry method on silicon substrate, in: Electronics, Communications and Photonics Conference (SIECPC), Saudi International, 2013, pp. 1–4.
[63] H. Yan, J. Yang, G. Ma, G. Wu, X. Zong, Z. Lei, J. Shi, C. Li, Visible-light-driven hydrogen production with extremely high quantum efficiency on Pt–PdS/CdS photocatalyst, J. Catal. 266 (2009) 165–168.
[64] O. Zelaya Angel, J.J. Alvarado Gil, R. LozadaMorales, H. Vargas, A. Ferreira da Silva, Band gap shift in CdS semiconductor by photoacoustic spectroscopy: evidence of a cubic to hexagonal lattice transition, Appl. Phys. Lett. 64 (1994) 291–293.
[65] J. J. Kim, J. Kim, D.-R. Jung Lee, H. Kim, H. Choi, S. Lee, S. Byun, S. Kang, Photoluminescence enhancement in CdS quantum dots by thermal annealing, Nanoscale Res. Lett. 7 (2012) 1–7.
[66] G.I.N. Waterhouse, M. Murdoch, J. Llorca, H. Idriss, Ethanol photoreaction to hydrogen over Au/TiO_2 catalysts. Investigating the synergistic effect of nanoparticles, Int. J. Nanotechnol. 9 (2012) 113–120.
[67] K. Connelly, A.K. Wahab, H. Idriss, Photoreaction of Au/TiO_2 for hydrogen production from renewables: a review on the synergistic effect between anatase and rutile phases of TiO_2, Mater. Renew. Sustain. Energy 1 (2012) 1–12.
[68] D. Lahiri, V. Subramanian, T. Shibata, E.E. Wolf, B.A. Bunker, P.V. Kamat, Photoinduced transformations at semiconductor/metal interfaces: X-ray absorption studies of titania/gold films, J. Appl. Phys. 93 (2003) 2575–2582.
[69] A.C. Templeton, J.J. Pietron, R.W. Murray, P. Mulvaney, Solvent refractive index and core charge influences on the surface plasmon absorbance of alkanethiolate monolayer-protected gold clusters, J. Phys. Chem. B 104 (1999) 564–570.
[70] X. H. Chen, Z. Kou, W. Yang, J. Wang Ni, Shape- and size-dependent refractive index sensitivity of gold nanoparticles, Langmuir 24 (2008) 5233–5237.
[71] M. Stoev, A. Katerski, XPS and XRD study of photoconductive CdS films obtained by a chemical bath deposition process, J. Mater. Chem. 6 (1996) 377–380.
[72] K.W. Kolasinski, Surface Science: Foundations of Catalysis and Nanoscience, 2nd ed., John Wiley & Sons, West Sussex PO19 8SQ, England, 2008.
[73] C.J. Nelin, P.S. Bagus, M.A. Brown, M. Sterrer, H.-J. Freund, Analysis of the broadening of X-ray photoelectron spectroscopy peaks for ionic crystals, Angew. Chem. Int. Ed. 50 (2011) 10174–10177.
[74] L. Ley, J. Reichardt, R. Johnson, Static charge fluctuations in amorphous silicon, Phys. Rev. Lett. 49 (1982) 1664.
[75] M.A. Nadeem, I. Majeed, G.I.N. Waterhouse, H. Idriss, Study of ethanol reactions on H_2 reduced Au/TiO_2 anatase and rutile: effect of metal loading on reaction selectivity, Catal. Struct. React. (2014) 61–700.
[76] J.B. Joo, R. Dillon, I. Lee, Y. Yin, C.J. Bardeen, F. Zaera, Promotion of atomic hydrogen recombination as an alternative to electron trapping for the role of metals in the photocatalytic production of H_2, Proc. Natl. Acad. Sci. 111 (2014) 7942–7947.
[77] M. Bowker, L. Millard, J. Greaves, D. James, J. Soares, Photocatalysis by Au nanoparticles: reforming of methanol, Gold Bull. 37 (2004) 170–173.
[78] M. Bowker, Sustainable hydrogen production by the application of ambient temperature photocatalysis, Green Chem. 13 (2011) 2235–2246.
[79] B. Wang, S. Qu, Absorption spectra and near-electric field enhancement effects of Au- and Ag–Fe_3O_4 dimers, Appl. Surf. Sci. 292 (2014) 1002–1008.
[80] S. Linic, P. Christopher, D.B. Ingram, Plasmonic-metal nanostructures for efficient conversion of solar to chemical energy, Nat. Mater. 10 (2011) 911–921.
[81] K. Yu, Y. Tian, T. Tatsuma, Size effects of gold nanaoparticles on plasmon-induced photocurrents of gold–TiO_2 nanocomposites, Phys. Chem. Chem. Phys. 8 (2006) 5417–5420.

[82] C. Clavero, Plasmon-induced hot-electron generation at nanoparticle/metal-oxide interfaces for photovoltaic and photocatalytic devices, Nat. Photonics 8 (2014) 95–103.
[83] Y. Zhang, C. Gu, A.M. Schwartzberg, S. Chen, J.Z. Zhang, Optical trapping and light-induced agglomeration of gold nanoparticle aggregates, Phys. Rev. B 73 (2006) 165405.
[84] O. Neumann, A.S. Urban, J. Day, S. Lal, P. Nordlander, N.J. Halas, Solar vapor generation enabled by nanoparticles, ACS Nano 7 (2013) 42–49.
[85] Z. Fang, Y.-R. Zhen, O. Neumann, A. Polman, F.J. García de Abajo, P. Nordlander, N.J. Halas, Evolution of light-induced vapor generation at a liquid-immersed metallic nanoparticle, Nano Lett. 13 (2013) 1736–1742.
[86] J.L. Sullivan, An ultrasonic identification of diffusion mechanisms in CdS, IEEE Trans. Ultrason. 32 (1985) 71–75.
[87] A. Janssen, S. Meijer, J. Bontsema, G. Lettinga, Application of the redox potential for controling a sulfide oxidizing bioreactor, Biotechnol. Bioeng. 60 (1998) 147–155.
[88] R. Vogel, P. Hoyer, H. Weller, Quantum-sized PbS, CdS, Ag_2S, Sb_2S_3, and Bi_2S_3 particles as sensitizers for various nanoporous wide-bandgap semiconductors, J. Phys. Chem. 98 (1994) 3183–3188.
[89] Z. Jin, Q. Li, X. Zheng, C. Xi, C. Wang, H. Zhang, L. Feng, H. Wang, Z. Chen, Z. Jiang, Surface properties of Pt/CdS and mechanism of photocatalytic dehydrogenation of aqueous alcohol, J. Photochem. Photobiol. A 71 (1993) 85–96.
[90] A.F. Singaevsky, Y.P. Piryatinski, D.O. Grynko, O.P. Dimitriev, Asymmetric effect of $(000\bar{1})$ and (0001) facets on surface and interface properties of CdS single crystal, Appl. Phys. A 104 (2011) 493–502.
[91] A.S. Barnard, H. Xu, First principles and thermodynamic modeling of CdS Surfaces and nanorods, J. Phys. Chem. C 111 (2007) 18112–18117.
[92] W.N. Unertle, Physical Structure, Elsevier Science B.V., Amsterdam, The Netherlands, 1996.
[93] W.H. Koppenol, J. Butler, Energetics of interconversion reactions of oxyradicals, Adv. Free Radical Biol. Med. 1 (1985) 91–131.
[94] R.T. Zehr, M.A. Henderson, Acetaldehyde photochemistry on TiO_2(110), Surf. Sci. 602 (2008) 2238–2249.
[95] T. Reztsova, C.-H. Chang, J. Koresh, H. Idriss, Dark- and photoreactions of ethanol and acetaldehyde over TiO_2/carbon molecular sieve fibers, J. Catal. 185 (1999) 223–235.
[96] J.N. Wilson, H. Idriss, Surface reconstruction of TiO_2(001) single crystal on the photoreaction of acetic acid, J.Catal. 214 (2003) 46–52.
[97] J.N. Wilson, H. Idriss, Structure-sensitivity and photo-catalytic reactions of semiconductors. Effect of the last layer atomic arrangement, J. Am. Chem. Soc. 124 (2002) 11284–11285.